RSC Advances

PAPER

View Article Online
View Journal | View Issue

Cite this: *RSC Adv.*, 2017, **7**, 42819

Enhanced photocatalytic CO_2 reduction over Co-doped NH_2-MIL-125(Ti) under visible light†

Yanghe Fu,[ab] Huan Yang,[a] Rongfei Du,[a] Gaomei Tu,[a] Chunhui Xu,[a] Fumin Zhang,[a] Maohong Fan*[b] and Weidong Zhu*[a]

Received 6th June 2017
Accepted 29th August 2017

DOI: 10.1039/c7ra06324e

rsc.li/rsc-advances

Co-doped NH_2-MIL-125(Ti) catalysts [Co/NH_2-MIL-125(Ti)] are developed for the photocatalytic reduction of CO_2 upon visible-light irradiation. Compared with NH_2-MIL-125(Ti), Co/NH_2-MIL-125(Ti) exhibits a significantly enhanced activity in CO_2 reduction, due to the fact that the doping of Co nanoparticles onto NH_2-MIL-125(Ti) can promote the visible-light harvesting and electron transfer. In addition, when benzylic alcohols as electron donors, instead of triethanolamine (TEOA) which is often used as a sacrificial agent, are added into the reaction system, Co/NH_2-MIL-125(Ti) can simultaneously catalyze CO_2 reduction to formic acid (HCOOH) and the selective oxidation of the benzylic alcohols to the corresponding aldehydes, making the proposed process more economical and environment-friendly.

1. Introduction

To solve the problems associated with both global warming and energy shortage, the conversion of CO_2 into valuable organic products utilizing renewable solar energy is considered as a promising approach.[1–3] Over the past four decades various photocatalysts, such as inorganic semiconductors, metal-incorporated zeolites, and metal complexes, have been developed for CO_2 reduction.[4–12] However, most of them are only active in an ultraviolet (UV) region and their efficiencies for CO_2 reduction and selectivities for the desired products are still quite low. Therefore, it would be of great importance to develop visible-light-responsive and highly efficient, selective photocatalysts for CO_2 reduction.

Metal–organic frameworks (MOFs), which have been extensively studied over the past two decades and shown a variety of applications in gas storage/separation, biomedicine, as well as heterogeneous catalysis,[13–20] could be promising candidates for photocatalytic CO_2 reduction. It has been reported that in MOFs the metal-oxo clusters could act as inorganic semiconducting quantum dots while the organic linkers serve as antennas to activate these semiconducting quantum dots by the ligand-to-metal charge transfer upon photoexcitation, thus making MOF-based photocatalysis possible.[21] In addition, MOFs are good at CO_2 capture due to their large surface area, high porosity, and tunable interactions with CO_2,[22] facilitating the photocatalytic reduction of CO_2. In fact, some investigators have demonstrated the applications of MOF-based photocatalysts in CO_2 reduction.[23–32] For example, Jiang *et al.* reported that a very stable mesoporous zirconium-porphyrin MOF, PCN-222, could selectively capture CO_2 and further photoreduce CO_2 with triethanolamine (TEOA) as a sacrificial agent upon visible-light irradiation.[23] Li *et al.* used series of photocatalysts based on UiO-66(Zr) in CO_2 reduction to formates upon visible-light irradiation in the presence of TEOA.[25–27] However, the activities of the reported MOF-based photocatalysts are still quite low and TEOA must be used as the sacrificial agent during CO_2 reduction, which is not economical and environment-friendly, due to the following reasons: (1) TEOA cannot be converted to valuable products, just as a sacrificial hole scavenger; (2) the excessive emission of TEOA will cause the environmental pollution; and (3) the use of TEOA will lead to the laborious purification of the produced HCOOH due to the strong intermolecular interactions between the formed acid–base adducts. It is therefore indispensable to enhance the activities of MOF-based photocatalysts and to find alternatives to avoid using sacrificial agents such as TEOA in photocatalytic CO_2 reduction. In our previous work, it was found that Ni-doped NH_2-MIL-125(Ti) could effectively catalyze the aerobic oxidation of benzylic alcohols to the corresponding aldehydes upon visible-light irradiation.[33] In addition, it is well known that benzylic alcohols can be used as electron donors.[34] Thus, it is anticipated that the doping of some metallic nanoparticles (NPs) into MOFs such as NH_2-MIL-125(Ti) might also enhance the photocatalytic activity in CO_2 reduction and simultaneously promote the selective oxidation of the benzylic alcohols used as electron donors. It would be highly desirable that the benzylic alcohols can be selectively oxidized into the corresponding aldehydes

[a]*Key Laboratory of the Ministry of Education for Advanced Catalysis Materials, Institute of Physical Chemistry, Zhejiang Normal University, Jinhua 321004, People's Republic of China. E-mail: weidongzhu@zjnu.cn; Fax: +86 579 82282932; Tel: +86 579 82282932*

[b]*Department of Chemical and Petroleum Engineering, University of Wyoming, Laramie, WY 82071, USA. E-mail: mfan@uwyo.edu; Fax: +1 307 7666777; Tel: +1 307 7665633*

† Electronic supplementary information (ESI) available. See DOI: 10.1039/c7ra06324e

during photocatalytic CO_2 reduction, because the produced aldehydes and their derivatives are important building blocks for producing fine chemicals.

Herein, for the first time, we developed metallic Co NPs doped NH_2-MIL-125(Ti) catalysts [Co/NH_2-MIL-125(Ti)] for photocatalytic CO_2 reduction using benzylic alcohols as electron donors upon visible-light irradiation. It's found that Co/NH_2-MIL-125(Ti) catalysts exhibit significantly enhanced activities in CO_2 reduction and benzylic alcohols could be oxidized to the corresponding aldehydes during photocatalytic CO_2 reduction. The effects of the doped Co NPs on the photocatalysis were investigated in detail and the possible photocatalytic mechanism for CO_2 reduction was proposed.

2. Experimental

2.1. Materials

All reagents with analytical reagent grade were used as received without further purification. Tetrabutyl titanate [$Ti(OC_4H_9)_4$], potassium bicarbonate ($KHCO_3$), triethanolamine (TEOA), acetonitrile (MeCN), acetonitrile-D3 (CD_3CN) and cobalt(II) nitrate hexahydrate [$Co(NO_3)_2 \cdot 6H_2O$] were purchased from Shanghai Chemical Reagent Co. 2-Amino-benzenedicarboxylic acid (H_2BDC-NH_2), methanol (MeOH) and dimethylformamide (DMF) were purchased from Sigma Aldrich Co. Sodium borohydride ($NaBH_4$), sodium carbonate (Na_2CO_3), sodium bicarbonate ($NaHCO_3$), benzotrifluoride (BTF), benzyl alcohol, 4-methoxybenzyl alcohol, benzaldehyde, and 4-methoxybenzaldehyde were purchased from Aladdin Industrial Co.

2.2. Synthesis

2.2.1. NH_2-MIL-125(Ti). Based on the recipe reported in the literature,[30] NH_2-MIL-125(Ti) was prepared *via* a hydrothermal treatment of H_2BDC-NH_2 (0.54 g, 3 mmol) and $Ti(OC_4H_9)_4$ (0.26 mL, 0.75 mmol) in the solvent of DMF (9 mL) and dry MeOH (1 mL) at 150 °C for 3 days. After hydrothermal treatment, the resultant suspension was filtered, washed with DMF and MeOH, extracted by a Soxhlet extractor with MeOH, and finally vacuum-dried to obtain the product.

2.2.2. Co/NH_2-MIL-125(Ti). The Co-doped NH_2-MIL-125(Ti) samples were prepared through solution infiltration of activated NH_2-MIL-125(Ti) with MeOH solution (0.5 mL) containing $Co(NO_3)_2 \cdot 6H_2O$. The mixture was stirred for 12 h, then filtered and dried at 150 °C for 3 h, followed by treatment with a $NaBH_4$ solution (20 mL, 0.05 M). The resulting solid powder was washed with MeOH and deionized water for several times and dried under N_2 atmosphere at 60 °C for 10 h to get Co/NH_2-MIL-125(Ti). The nominal doped amounts of Co in NH_2-MIL-125(Ti) were 1.0, 2.0, and 3.0 wt%, denoted as 1.0 wt% Co/NH_2-MIL-125(Ti), 2.0 wt% Co/NH_2-MIL-125(Ti), and 3.0 wt% Co/NH_2-MIL-125(Ti), respectively.

2.3. Characterization

X-ray powder diffraction (XRD) patterns were collected on a Philips PW3040/60 diffractometer using Cu Kα radiation (λ = 0.1541 nm) in a scanning range of 5–50° at 1° min^{-1}. After digestion of Co/NH_2-MIL-101(Ti) (0.05 g) in a solution of 2 mL HF (40 wt%) and 8 mL H_2SO_4 (98 wt%) diluted to 100 mL with deionized water, the Co loadings of the prepared catalysts were determined by an IRIS Intrepid IIXSP inductively coupling plasma-atomic emission spectrometer (ICP-AES). The Brunauer–Emmett–Teller (BET) surface areas of the prepared samples were determined by N_2 adsorption/desorption at −196 °C using a Micromeritics ASAP 2020 instrument. The samples were degassed in vacuum at 150 °C for 12 h before the adsorption measurement. The UV-vis diffuse reflectance spectra (UV-vis DRS) of the samples were recorded on a Shimadzu UV-3600 spectrophotometer from 200 nm to 800 nm. The scanning electron microscope (SEM) was carried out on a Hitachi S-4800 apparatus equipped with a field emission gun. The high resolution transmission electron microscopy (HR-TEM) was conducted on a JEOL JEM-1200 working at 200 kV. The X-ray photoelectron spectroscopy (XPS) was carried out on Thermo Scientific EscaLab 250Xi using Al Kα radiation. The ^{13}C nuclear magnetic resonance (NMR) was carried out on a Bruker AVANCE III 500M system (500 MHz). The isotopic $^{13}CO_2$ reduction was performed in an NMR tube filled with photocatalyst in a CD_3CN/TEOA (5 : 1 v/v) solution. The spectrum was recorded under the following conditions: acquisition time 1.0 s, 20 000 times integration. The electron spin resonance (ESR) spectra were obtained over Bruker ESP 300 E electron paramagnetic resonance spectrometer at room temperature. The photoluminescence (PL) spectra were recorded on a Hitachi F-7000 spectrometer. The photocurrent (PC) analysis was carried out with a CHI440A workstation (Shanghai Chenhua Instruments Co.) in a conventional three-electrode cell using a Pt plate and an Ag/AgCl electrode as the counter electrode and reference electrode, respectively. The photocatalyst powder deposited on the fluoride tin oxide (FTO) substrate was employed as the working electrode and a quartz cell filled with 100 mL 0.2 M Na_2SO_4 electrolyte was used as the reaction system. A 300 W xenon lamp (Beijing Perfectlight, PLS-SXE 300c) system was applied as the excitation light source equipped with a UV cutoff filter, which was the same light source for the photocatalytic tests. The Mott–Schottky curves were measured using a ZENNIUM electrochemical analyzer (Zahner, Germany) in a three-electrode cell. Pt plate and Ag/AgCl electrode (3 M KCl) were used as the counter and reference electrode, respectively. The electrolyte was a 0.2 M aqueous solution of Na_2SO_4 without additive and was purged with N_2 gas for 2 h prior to the measurements. The potential ranged from −0.3 V to 0.8 V (*vs.* Ag/AgCl), and the perturbation signal was 20 mV with the frequency from 500 Hz to 1500 Hz. The working electrodes were immersed in the electrolyte for 60 s before any measurement was taken.

2.4. Photocatalytic reaction

Prior to photocatalytic reactions, the catalysts were treated under vacuum at 150 °C to remove any adsorbed impurities. 50 mg of the photocatalyst was degassed and purged with CO_2. A mixture of MeCN and TEOA with a volume ratio of 5 to 1 and a total volume of 60 mL, degassed by CO_2 to remove dissolved

O_2, was injected into the reaction flask. The photocatalytic reaction was carried out under the irradiation of a 300 W Xe lamp with a UV-cut filter and an IR-cut filter (800 nm $\geq \lambda \geq$ 420 nm). The formed HCOOH was detected by ion chromatography (930 Compact IC pro, Metrosep) with a Metrosep A Supp 5 250/4.0 column. A mixture of 3.2 mM Na_2CO_3 and 1.0 mM $NaHCO_3$ was used as eluent. The gaseous reaction products were also analyzed using a GC-FID (Agilent 6890A) with a HP-5 capillary column.

When benzylic alcohols instead of TEOA were used as electron donors, $KHCO_3$ (50 mg) was added to provide a basic environment for facilitating photocatalytic CO_2 reduction. The volume ratio of MeCN to the benzylic alcohol was 10 to 1 with a total volume of 110 mL.

For the reusability test, the photocatalyst was separated from the reaction medium after the first run, repeatedly washed with MeOH three times, and then dried overnight in a vacuum oven at 150 °C. Then, the dried catalyst was used in the next run.

3. Results and discussion

3.1. Characterization

Co/NH_2-MIL-125(Ti) samples were prepared by an impregnation of the activated NH_2-MIL-125(Ti) with $[Co(NO_3)_2 \cdot 6H_2O]$ solution, reduced by an aqueous $NaBH_4$ solution. The physiochemical properties of the prepared catalysts are summarized in Table 1. The doped amounts of Co NPs on NH_2-MIL-125(Ti) determined by the ICP-AES analysis were 0.91, 1.97, and 2.91 wt%, respectively, well corresponding to their nominal values in the synthesis. In comparison with NH_2-MIL-125(Ti), the BET surface areas and the pore volumes of Co/NH_2-MIL-125(Ti) tend to decrease gradually with increasing Co doping in the matrix of NH_2-MIL-125(Ti), due to the fact that the cages of NH_2-MIL-125(Ti) are occupied by the dispersed Co NPs and/or blocked by the Co NPs that could partially be deposited at the pore entrances of the MOF. Fig. 1 shows that the XRD patterns of Co/NH_2-MIL-125(Ti) are almost the same as that of NH_2-MIL-125(Ti), indicating that the doping of Co on NH_2-MIL-125(Ti) does not influence its crystallinity. Additionally, no characteristic peak of Co species can be observed due to the low loading amount and high dispersion of Co on the MOF. The SEM images (Fig. 2) display that the morphologies of the Co-doped samples are the same as that of NH_2-MIL-125, indicating that the structure of NH_2-MIL-125 is well preserved. The sizes of the

Table 1 Physiochemical properties of the prepared catalysts

Catalyst	Co loading[a] wt%	S_{BET} $m^2\ g^{-1}$	$S_{Langmuir}$ $m^2\ g^{-1}$	V_{total} $cm^3\ g^{-1}$
NH_2-MIL-125	—	1132	1586	0.65
1.0 wt% NH_2-MIL-125	0.91	926	1360	0.57
2.0 wt% NH_2-MIL-125	1.97	824	1214	0.54
3.0 wt% NH_2-MIL-125	2.98	765	1123	0.53

[a] The doped amounts of Co in NH_2-MIL-125(Ti) were determined by the ICP-AES analysis.

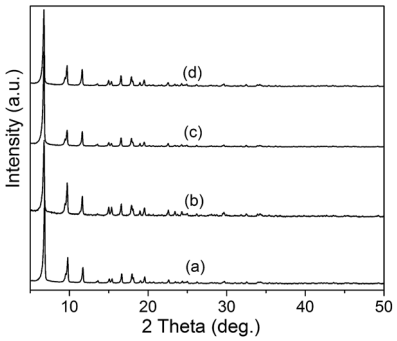

Fig. 1 XRD patterns of NH_2-MIL-125(Ti) (a), 1.0 wt% Co/NH_2-MIL-125(Ti) (b), 2.0 wt% Co/NH_2-MIL-125(Ti) (c), and 3.0 wt% Co/NH_2-MIL-125(Ti) (d).

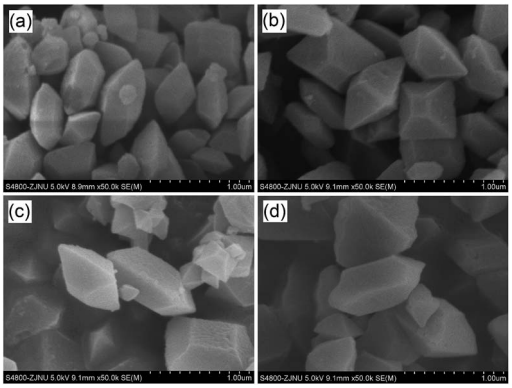

Fig. 2 SEM images of NH_2-MIL-125(Ti) (a), 1.0 wt% Co/NH_2-MIL-125(Ti) (b), 2.0 wt% Co/NH_2-MIL-125(Ti) (c), and 3.0 wt% Co/NH_2-MIL-125(Ti) (d).

Co NPs doped on NH_2-MIL-125(Ti) have a mean diameter of 5 nm from the TEM observation, as shown in Fig. 3. The HR-TEM images of Co/NH_2-MIL-125(Ti) samples show the characteristic spacings of 0.177 and 0.205 nm for the (2 0 0) and the (1 1 1) lattice planes of cubic Co (JCPDS, no. 15-0806), and the characteristic spacings of 0.213 and 0.246 nm for the (2 0 0) and (1 1 1) lattice planes of CoO (JCPDS, no. 48-1719), respectively. In order

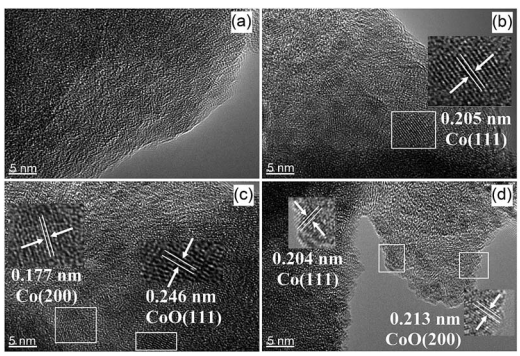

Fig. 3 HR-TEM images of NH_2-MIL-125(Ti) (a), 1.0 wt% Co/NH_2-MIL-125(Ti) (b), 2.0 wt% Co/NH_2-MIL-125(Ti) (c), and 3.0 wt% Co/NH_2-MIL-125(Ti) (d).

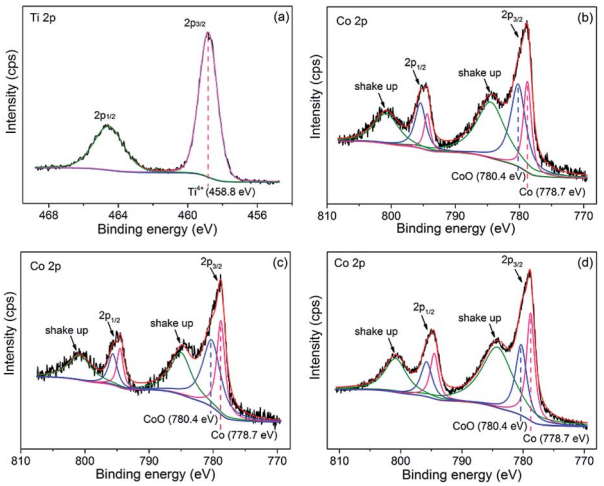

Fig. 4 High-resolution XPS spectra for Co 2p of NH_2-MIL-125(Ti) (a), 1.0 wt% Co/NH_2-MIL-125(Ti) (b), 2.0 wt% Co/NH_2-MIL-125(Ti) (c), and 3.0 wt% Co/NH_2-MIL-125(Ti) (d).

to confirm the results from HR-TEM, the X-ray photoelectron spectroscopy was used to characterize the Co oxidation state (Fig. 4). The coexistence of the metallic and oxidized Co in Co/NH_2-MIL-125(Ti) is evidenced by two peaks of Co $2p_{3/2}$ located at 778.7 and 780.4 eV, which are assigned to Co^0 and Co^{2+}.[35] The oxidized Co could be ascribed to the partial oxidation when the Co NPs in Co/NH_2-MIL-125(Ti) are exposed to the atmosphere since they are very active to be oxidized. It's generally accepted that their activity tends to increase with declining their particle size.[36] As can be seen from Fig. 5, the UV-vis spectra of both NH_2-MIL-125(Ti) and Co/NH_2-MIL-125(Ti) show a similar absorption onset (*ca.* 505 nm), thereby suggesting an optical band gap of ~2.5 eV as determined by the Kubelka–Munk function. However, the UV-vis spectra of Co/NH_2-MIL-125(Ti) show an extra absorption band in the visible-light region ranging from 500 to 800 nm, compared with NH_2-MIL-125(Ti), in accordance with their dark green color changed from yellow. The enhanced visible-light harvesting would be of great importance in photocatalysis and thus Co/NH_2-MIL-125(Ti) catalysts are expected to possess better photocatalytic activities toward target reactions.

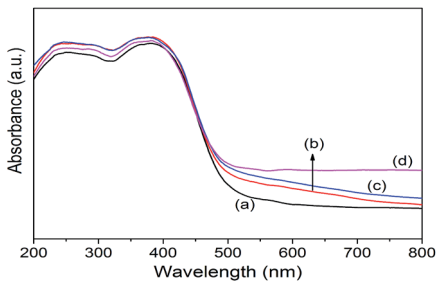

Fig. 5 UV-vis diffuse reflectance spectra of NH_2-MIL-125(Ti) (a), 1.0 wt% Co/NH_2-MIL-125(Ti) (b), 2.0 wt% Co/NH_2-MIL-125(Ti) (c), and 3.0 wt% Co/NH_2-MIL-125(Ti) (d).

3.2. Photocatalytic performance

3.2.1. Photocatalytic CO_2 reduction using TEOA as the sacrificial agent. To investigate the effects of the doped Co NPs on the photocatalytic performance, photocatalytic CO_2 reduction was carried out using TEOA as the sacrificial agent upon visible-light irradiation. No reaction took place in dark or without catalyst. Both NH_2-MIL-125(Ti) and Co/NH_2-MIL-125(Ti) can catalyze the reduction of CO_2 into HCOOH upon visible-light irradiation. A concentration change of HCOOH with irradiation time over the prepared photocatalysts is shown in Fig. 6. Compared to the photocatalytic activity of NH_2-MIL-125(Ti), Co/NH_2-MIL-125(Ti) catalysts are more active in CO_2 reduction. The effects of the Co content in the MOF on the photocatalytic performance were also examined. One can see that the optimum content of Co in NH_2-MIL-125(Ti) is about 1.0 wt% for photocatalytic CO_2 reduction with about 38.4 μmol g_{cat}^{-1} h^{-1} of the HCOOH produced in 10 h irradiation, since the excessive Co in the MOF may cause the blocking of the MOF pores to reduce the photoexciting capacity of NH_2-MIL-125(Ti). The isotopic $^{13}CO_2$ reaction was used to confirm that the produced HCOOH originated from CO_2. The ^{13}C NMR spectrum (Fig. S1 in the ESI†) shows three peaks at 125.76, 159.56, and 165.29 ppm, which can be assigned to dissolved CO_2, HCO_3^-, and HCOOH, respectively.[24] This indicates that the produced HCOOH originates from CO_2. In addition, the control experiments using cobalt(II) salt or CoO mixed with NH_2-MIL-125(Ti) as the photocatalyst were carried out in order to verify which Co species (metallic or Co^{2+}) would play a role in the reaction, see Table S1 in the ESI.† The amount of the HCOOH produced in the presence of cobalt(II) salt or CoO-mixed with NH_2-MIL-125(Ti) (entries 2 and 3) is almost the same as that over NH_2-MIL-125(Ti) (entry 1), indicating that the enhanced activity of Co/NH_2-MIL-125(Ti) results from the Co NPs but not from the Co oxidized species.

3.2.2. Aerobic oxidation of benzylic alcohols. In our previous study, it was found that Ni-doped NH_2-MIL-125(Ti)

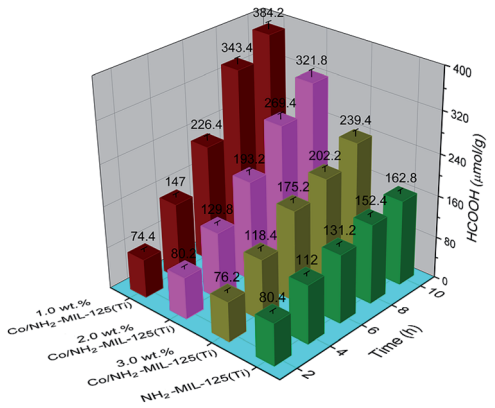

Fig. 6 Amount of the produced HCOOH as a function of irradiation time over NH_2-MIL-125(Ti), 1.0 wt% Co/NH_2-MIL-125(Ti), 2.0 wt% Co/NH_2-MIL-125(Ti), and 3.0 wt% Co/NH_2-MIL-125(Ti). The solutions were irradiated with a Xe lamp and filters producing light in a range of 420–800 nm. Photocatalyst: 50 mg, MeCN/TEOA volume ratio: 5/1, total solution volume: 60 mL.

Table 2 Aerobic photocatalytic oxidation of benzylic alcohols to the corresponding aldehydes over 1 wt% Co/NH_2-MIL-125(Ti) upon visible-light irradiation[a]

Entry	Catalyst	Benzylic alcohol	Conversion (%)	Selectivity (%)
1	NH_2-MIL-125(Ti)	Benzyl alcohol	12.5	>99
2		4-Methoxybenzyl alcohol	42.5	>99
3	1 wt% Co/NH_2-MIL-125(Ti)	Benzyl alcohol	23.9	>99
4		4-Methoxybenzyl alcohol	50.6	>99

[a] Reaction conditions: 50 mg of catalyst and 0.3 mmol of benzylic alcohol in 6 mL of BTF at room temperature for 10 h.

shows an enhanced photocatalytic activity in the selective oxidation of benzylic alcohols to the corresponding aldehydes.[33] Herein, the aerobic oxidation of benzylic alcohols over Co/NH_2-MIL-125(Ti) was also investigated, and these results are summarized in Table 2. Remarkably, compared with NH_2-MIL-125(Ti), Co/NH_2-MIL-125(Ti) shows an enhanced activity for the oxidation of benzyl alcohol and 4-methoxybenzyl alcohol with high selectivity (>99%). The conversions of the benzylic alcohols over Co/NH_2-MIL-125(Ti) are even higher than those over Ni/NH_2-MIL-125(Ti), implying that the electron transfer is more effective for the doping of the Co NPs into NH_2-MIL-125(Ti).

3.2.3. Photocatalytic CO_2 reduction coupled with oxidation of benzylic alcohols. Because TEOA as the sacrificial electron donor is not economical and environment-friendly while benzylic alcohols can be used as electron donors, we therefore carried out photocatalytic CO_2 reduction with the oxidation of benzylic alcohols. These results are summarized in Table 3. $KHCO_3$ was added into the reaction medium in order to provide a basic environment for facilitating the photocatalytic reduction. When benzyl alcohol was used as the electron donor, no product was detected over NH_2-MIL-125(Ti) upon visible-light irradiation for 10 h. On the contrary, the yields of benzaldehyde and HCOOH over 1.0 wt% Co/NH_2-MIL-125(Ti) under the same conditions were 2.2 and 2.4 μmol g_{cat}^{-1} h^{-1} (entries 1 and 3), respectively. In case of 4-methoxybenzyl alcohol, 4-methoxybenzaldehyde and HCOOH were formed over both NH_2-MIL-125(Ti) and 1.0 wt% Co/NH_2-MIL-125(Ti) catalysts (entries 2 and 4), and the yields of 4-methoxybenzaldehyde and HCOOH over 1.0 wt% Co/NH_2-MIL-125(Ti) were up to 5.8 and 6.0 μmol g_{cat}^{-1} h^{-1}. It is undoubted that the electron donating substituent on the phenyl ring is favorable for the photocatalytic reaction. It has been reported that the photocatalytic activity can be enhanced if the catalyst is made more electron conductive.[37,38] Although there is still the lack of thorough understanding on the photocatalytically active sites, it is proposed that the enhanced catalytic activity might come from the electronic interactions between the Co NPs and NH_2-MIL-125(Ti).

3.2.4. Reusability. A six-run experiment of photocatalytic CO_2 reduction with TEOA as the sacrificial agent was carried out to check the reusability of 1 wt% Co/NH_2-MIL-125(Ti) as an illustrative example, as shown in Fig. S2 in the ESI.† Obviously, the recycling use of the photocatalyst for six runs shows no obvious decrease of the photocatalytic activity. In addition, the XRD, FT-IR, N_2 adsorption–desorption, and XPS characterization results for the photocatalyst after the 6th-run reaction are almost identical to those for the fresh one (Fig. S3 in the ESI†), suggesting that the prepared catalyst is stable during the photocatalytic reaction. In addition, the photocatalytic reduction of CO_2 upon UV irradiation was carried out to further check the stability of 1 wt% Co/NH_2-MIL-125(Ti), and the corresponding results are shown in Fig. S4 in the ESI,† in which there is no obvious decrease in the photocatalytic activity for six runs. Moreover, the results from the XRD, N_2 adsorption–desorption, and FT-IR characterizations of the photocatalyst after the 6th-run reaction are almost the same as those for the fresh one (Fig. S5 in the ESI†), indicating that the photocatalyst is stable upon UV-light irradiation.

3.3. Mechanism for photocatalytic CO_2 reduction

To elucidate the semiconducting properties of NH_2-MIL-101(Ti) upon light excitation, the Mott–Schottky method was applied to estimate the flat band positions of the photocatalysts, because it is a generally accepted method in the determination of the flat band positions of semiconductors.[39,40] The flat band positions for NH_2-MIL-125(Ti) and 1.0 wt% Co/NH_2-MIL-125(Ti) were determined to be −0.40 V and −0.43 V *vs.* NHE, respectively (Fig. S6 in the ESI†). As observed from the Mott–Schottky measurements, both NH_2-MIL-125(Ti) and 1.0 wt% Co/NH_2-MIL-125(Ti) have characteristics of n-type semiconductors, therefore their conduction band (CB) positions should be close to their flat band ones. A comparable position observed for the conduction bands of NH_2-MIL-125(Ti) and Co/NH_2-MIL-125(Ti) indicates that the introduction of Co NPs does not influence the conduction band, implying that the photo-generated electrons

Table 3 Photocatalytic reduction of CO_2 coupled with oxidation of different benzylic alcohols[a]

Entry	Catalyst	Benzylic alcohol	Benzylic aldehyde (μmol g_{cat}^{-1} h^{-1})	HCOOH (μmol g_{cat}^{-1} h^{-1})
1	NH_2-MIL-125(Ti)	Benzyl alcohol	n.d.[b]	n.d.
2		4-Methoxybenzyl alcohol	4.6	4.8
3	1 wt% Co/NH_2-MIL-125(Ti)	Benzyl alcohol	2.2	2.3
4		4-Methoxybenzyl alcohol	5.8	6.0

[a] Reaction conditions: 50 mg of photocatalyst, a MeCN/benzylic alcohol volume ratio of 10 to 1, a total solution volume of 110 mL upon visible-light irradiation (800 nm ≥ λ ≥ 420 nm) for 10 h. [b] n.d.: not detect.

could be located at the metal centers in these MOFs. The CB position is more negative than the reduction potential of CO_2 to form HCOOH (−0.28 V *vs.* NHE),[41] indicating that Co/NH_2-MIL-101(Ti) can reduce CO_2 to form HCOOH (Fig. S7 in the ESI†). Although the doping of Co NPs into NH_2-MIL-125(Ti) could not affect its energy band structure, it could promote the photo-generated charge separation efficiency, which is confirmed by the PL and PC experiments. Fig. 7 shows the PL spectra of NH_2-MIL-125(Ti) and Co/NH_2-MIL-125(Ti) excited at 303 nm. NH_2-MIL-125(Ti) exhibits a PL peak at around 449 nm, and such a peak is greatly weakened upon being doped with Co NPs, indicating that Co/NH_2-MIL-125(Ti) can significantly prohibit the photo-generated charge recombination. The interactions between Co NPs and NH_2-MIL-125(Ti) can create a new way to extend the service life of photo-generated charge carriers *via* facilitating the electron transfer through Co NPs.[42] Electron cannot return from the excited state to the ground state, thus directly weakens the PL intensity of NH_2-MIL-125(Ti). The transient photocurrent density responses of the catalysts in an on–off cycle mode are shown in Fig. 8. Upon visible-light irradiation, all Co/NH_2-MIL-125(Ti) catalysts show much higher photoelectric currents in comparison with NH_2-MIL-125(Ti), among which 1.0 wt% Co/NH_2-MIL-125(Ti) exhibits the best photocurrent response. Based on these results, it can be

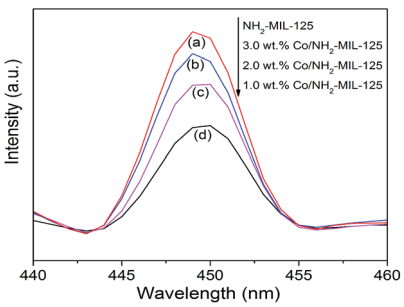

Fig. 7 Photoluminescence spectra of NH_2-MIL-125(Ti) (a), 3.0 wt% Co/NH_2-MIL-125(Ti) (b), 2.0 wt% Co/NH_2-MIL-125(Ti) (c), and 1.0 wt% Co/NH_2-MIL-125(Ti) (d) excited at 303 nm.

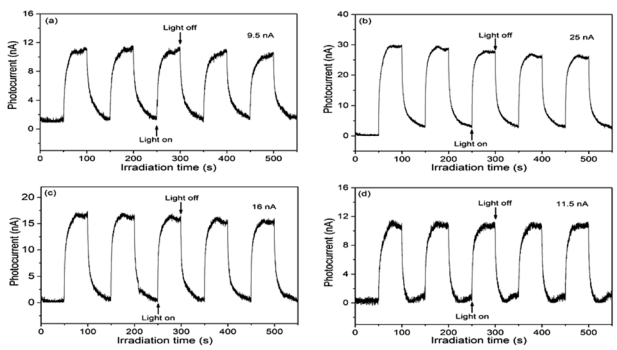

Fig. 8 Transient photocurrent responses of NH_2-MIL-125(Ti) (a), 1.0 wt% Co/NH_2-MIL-125(Ti) (b), 2.0 wt% Co/NH_2-MIL-125(Ti) (c), and 3.0 wt% Co/NH_2-MIL-125(Ti) (d) in 0.2 M Na_2SO_4 aqueous solution without bias *versus* Ag/AgCl upon visible-light irradiation (800 nm ≥ λ ≥ 420 nm).

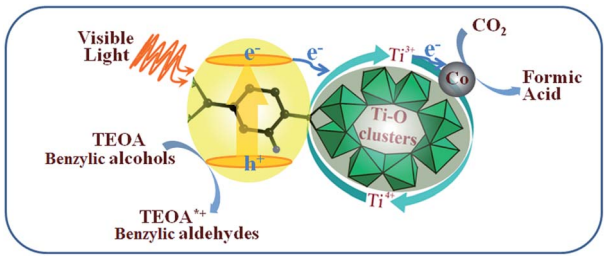

Scheme 1 Proposed mechanism for photocatalytic CO_2 reduction over Co/NH_2-MIL-125(Ti) upon visible-light irradiation.

inferred that the doping of Co NPs into NH_2-MIL-125(Ti) could facilitate photo-induced charge transfer and restrain the recombination of photo-generated charge efficiently, resulting in the higher photocatalytic activity in CO_2 reduction. The *in situ* ESR experiment was also carried out to detect the active species involved in the photocatalytic reaction, as shown in Fig. S8 in the ESI.† A signal assignable to Ti^{3+} species is observed in the ESR spectrum of Co/NH_2-MIL-101(Ti) after visible-light irradiation.[34] When CO_2 is introduced into the reaction system, the signal in the ESR spectrum corresponding to Ti^{3+} species disappears, indicating the reoxidation of generated Ti^{3+} species to Ti^{4+} species.

Herein, a mechanism for the enhancement of the photocatalytic reduction over Co/NH_2-MIL-125(Ti) was proposed, see Scheme 1. The excited ligands can transfer electrons to Ti oxo-clusters to form Ti^{3+} moieties upon visible-light irradiation, as termed linker-to-cluster charge-transfer (LCCT). The as-formed Ti^{3+} can reduce CO_2 into HCOOH in the presence of TEOA or benzylic alcohols acting as electron and hydrogen donors to achieve a complete photocatalytic cycle. When Co NPs are introduced into NH_2-MIL-125(Ti), they can also accept the electrons from the excited ligands, because Co NPs are usually good at electron traps. Meanwhile, the as-produced H atoms from TEOA or benzylic alcohols can spill over from the Co NPs to the bridging oxygen next to the Ti–O oxo-clusters and donate electrons to reduce Ti^{4+} to form Ti^{3+}. TEOA or the benzylic alcohols would be converted into TEOA^{*+} or the aldehydes by a de-protonation process during CO_2 reduction. Thus, the more efficient light-harvesting and charge-transfer of Co/NH_2-MIL-125(Ti) lead to a higher photocatalytic activity.

4. Conclusions

The photocatalytic reduction of CO_2 over Co/NH_2-MIL-125(Ti) upon visible-light irradiation has been fully investigated. Compared with NH_2-MIL-125(Ti), Co/NH_2-MIL-125(Ti) catalysts exhibit significantly enhanced activities for the photocatalytic reduction. In addition, the benzylic alcohols instead of TEOA used as elector donors can be oxidized to the corresponding aldehydes during the photocatalytic reduction of CO_2 over Co/NH_2-MIL-125(Ti), making the proposed process more economical and environment-friendly. Although the photocatalytic activity for CO_2 reduction coupled with the oxidation of benzylic alcohols over Co/NH_2-MIL-125(Ti) is still low, the current study

provides a novel way to convert CO_2 into valuable chemicals coupled with other organic transformations. Additionally, the elucidation of the mechanism on photocatalytic CO_2 reduction over Co/NH_2-MIL-125(Ti) provides some guidance in the development of high-efficient and visible-light-responsive photocatalysts based on MOF materials.

Conflicts of interest

There are no conflicts to declare.

Acknowledgements

We are grateful for the financial support by the National Natural Science Foundation of China (21303166, 21476214, and 21576243).

References

1 W. Wang, M. O. Tadé and Z. Shao, *Chem. Soc. Rev.*, 2015, **44**, 5371–5408.
2 P. Lanzafame, G. Centi and S. Perathoner, *Chem. Soc. Rev.*, 2014, **43**, 7562–7580.
3 X. Lang, X. Chen and J. Zhao, *Chem. Soc. Rev.*, 2014, **43**, 473–486.
4 G. Qin, Y. Zhang, X. Ke, X. Tong, Z. Sun, M. Liang and S. Xue, *Appl. Catal., B*, 2013, **129**, 599–605.
5 Y. Wang, Q. Lai, F. Zhang, X. Shen, M. Fan, Y. He and S. Ren, *RSC Adv.*, 2014, **4**, 44442–44451.
6 Y. He, L. Zhang, B. Teng and M. Fan, *Environ. Sci. Technol.*, 2015, **49**, 649–656.
7 Y. He, Y. Wang, L. Zhang, B. Teng and M. Fan, *Appl. Catal., B*, 2015, **168–169**, 1–8.
8 N. Linares, A. M. Silvestre-Albero, E. Serrano, J. Silvestre-Albero and J. García-Martínez, *Chem. Soc. Rev.*, 2014, **43**, 7681–7717.
9 J. Rongé, T. Bosserez, D. Martel, C. Nervi, L. Boarino, F. Taulelle, G. Decher, S. Bordiga and J. A. Martens, *Chem. Soc. Rev.*, 2014, **43**, 7963–7981.
10 W. Tu, Y. Zhou and Z. Zou, *Adv. Mater.*, 2014, **26**, 4607–4626.
11 W. Lin and H. Frei, *J. Am. Chem. Soc.*, 2005, **127**, 1610–1611.
12 S. Sato, T. Morikawa, T. Kajino and O. Ishitani, *Angew. Chem., Int. Ed.*, 2013, **125**, 1022–1026.
13 H. Furukawa, K. E. Cordova, M. O'Keeffe and O. M. Yaghi, *Science*, 2013, **341**, 1230444.
14 H.-C. Zhou and S. Kitagawa, *Chem. Soc. Rev.*, 2014, **43**, 5415–5418.
15 T. R. Cook, Y.-R. Zheng and P. J. Stang, *Chem. Rev.*, 2013, **113**, 734–777.
16 L. J. Murray, M. Dincă and J. R. Long, *Chem. Soc. Rev.*, 2009, **38**, 1294–1314.
17 J.-R. Li, J. Sculley and H.-C. Zhou, *Chem. Rev.*, 2012, **112**, 869–932.
18 P. Horcajada, R. Gref, T. Baati, P. K. Allan, G. Maurin, P. Couvreur, G. Férey, R. E. Morris and C. Serre, *Chem. Rev.*, 2012, **112**, 1232–1268.
19 A. Corma, H. García, F. X. Llabrés and I. Xamena, *Chem. Rev.*, 2010, **110**, 4606–4655.
20 L. Ma, C. Abney and W. Lin, *Chem. Soc. Rev.*, 2009, **38**, 1248–1256.
21 T. Tachikawa, J. R. Choi, M. Fujitsuka and T. Majima, *J. Phys. Chem. C*, 2008, **112**, 14090–14101.
22 K. Sumida, D. L. Rogow, J. A. Mason, T. M. McDonald, E. D. Bloch, Z. R. Herm, T.-H. Bae and J. R. Long, *Chem. Rev.*, 2012, **112**, 724–781.
23 H.-Q. Xu, J. Hu, D. Wang, Z. Li, Q. Zhang, Y. Luo, S.-H. Yu and H.-L. Jiang, *J. Am. Chem. Soc.*, 2015, **137**, 13440–13443.
24 D. Wang, R. Huang, W. Liu, D. Sun and Z. Li, *ACS Catal.*, 2014, **4**, 4254–4260.
25 D. Sun, Y. Fu, W. Liu, L. Ye, D. Wang, L. Yang, X. Fu and Z. Li, *Chem.–Eur. J.*, 2013, **19**, 14279–14285.
26 D. Sun, W. Liu, M. Qiu, Y. Zhang and Z. Li, *Chem. Commun.*, 2015, **51**, 2056–2059.
27 Y. Lee, S. Kim, J. K. Kang and S. M. Cohen, *Chem. Commun.*, 2015, **51**, 5735–5738.
28 S. Zhang, L. Li, S. Zhao, Z. Sun and J. Luo, *Inorg. Chem.*, 2015, **54**, 8375–8379.
29 C. Wang, Z. Xie, K. E. deKrafft and W. Lin, *J. Am. Chem. Soc.*, 2011, **133**, 13445–13454.
30 Y. Fu, D. Sun, Y. Chen, R. Huang, Z. Ding, X. Fu and Z. Li, *Angew. Chem., Int. Ed.*, 2012, **51**, 3364–3367.
31 L. Shi, T. Wang, H. Zhang, K. Chang and J. Ye, *Adv. Funct. Mater.*, 2015, **25**, 5360–5367.
32 D. Sun, W. Liu, Y. Fu, Z. Fang, F. Sun, X. Fu, Y. Zhang and Z. Li, *Chem.–Eur. J.*, 2014, **20**, 4780–4788.
33 Y. Fu, L. Sun, H. Yang, L. Xu, F. Zhang and W. Zhu, *Appl. Catal., B*, 2016, **187**, 212–217.
34 M. Dan-Hardi, C. Serre, T. Frot, L. Rozes, G. Maurin, C. Sanchez and G. Férey, *J. Am. Chem. Soc.*, 2009, **131**, 10857–10859.
35 H. Jin, J. Wang, D. Su, Z. Wei, Z. Pang and Y. Wang, *J. Am. Chem. Soc.*, 2015, **137**, 2688–2694.
36 P. Bazylewski, D. W. Boukhvalov, A. I. Kukharenko, E. Z. Kurmaev, A. Hunt, A. Moewes, Y. H. Lee, S. O. Cholakh and G. S. Chang, *RSC Adv.*, 2015, **5**, 75600–75606.
37 H. Fei, Y. Yang, Z. Peng, G. Ruan, Q. Zhong, L. Li, E. L. G. Samuel and J. M. Tour, *ACS Appl. Mater. Interfaces*, 2015, **7**, 8083–8087.
38 L. Wu, Q. Li, C. H. Wu, H. Zhu, A. Mendoza-Garcia, B. Shen, J. Guo and S. Sun, *J. Am. Chem. Soc.*, 2015, **137**, 7071–7074.
39 A. Ishikawa, T. Takata, J. N. Kondo, M. Hara, H. Kobayashi and K. Domen, *J. Am. Chem. Soc.*, 2002, **124**, 13547–13553.
40 A. Wolcott, W. A. Smith, T. R. Kuykendall, Y. Zhao and J. Z. Zhang, *Small*, 2009, **5**, 104–111.
41 V. P. Indrakanti, J. D. Kubicki and H. H. Schobert, *Energy Environ. Sci.*, 2009, **2**, 745–758.
42 G. Li, L. Wu, F. Li, P. Xu, D. Zhang and H. Li, *Nanoscale*, 2013, **5**, 2118–2125.